Development of human papillomavirus oral buccal mucosa microneedle vaccine

Kim, ChaiWon

Department of Medical Science
The Graduate School
Yonsei University

Development of human papillomavirus oral buccal mucosa microneedle vaccine

Advisor Kwak, Kihyuck

A Master's Thesis Submitted
to the Department of Medical Science
and the Committee on Graduate School
of Yonsei University in partial fulfillment of the
Requirements for the Degree of
Master of Medical Science

Kim, ChaiWon

July 2025

Development of human papillomavirus oral buccal mucosa microneedle vaccine

This Certifies that the Master's Thesis of Kim, ChaiWon is Approved

Committee Chair Lee, June-Yong

Committee Member Kwak, Kihyuck

Committee Member Kim, Jun-Seob

Department of Medical Science

The Graduate School

Yonsei University

July 2025

ACKNOWLEDGEMENTS

Though three years of my master's course felt long at times, I still feel there is much more for me to learn as I graduate. I would like to express my gratitude to my advisor, Professor Kihyuck Kwak for his guidance through my academic journey. I would extend thankfulness to Professor June-Yong Lee and Professor Jun-Seob Kim, for their thoughtful feedback and support as thesis committee members.

I feel lucky to have shared this time with lab members who walked alongside through both difficult and rewarding moments. I especially thank Dr. Hyemi Kim whose patient and reliable mentorship made my graduation possible. I'm also thankful to Ara, Minhee, Youngjae, Seungyong, Inhyuk and Hanseok for their support.

I'm deeply thankful to Siyoon and Hyeyeong who have been my unwavering supporters since my undergraduate years. Thank you for reminding me of my worth and giving me strength in the moments of doubt.

None of these would have been possible without my family. Thanks to my parents, JinNam Kim and ShookYoung Lee, and Yul Kim for cheering and supporting me unconditionally on from afar. I also want to thank my uncle JongSang Lee, aunt Boae Won, and cousins Yooho Lee and Sehwa Hong who helped me feel grounded and at home here in Korea

TABLE OF CONTENTS

LIST OF FIGURES

ABSTRACT

Development of human papillomavirus oral buccal mucosa microneedle vaccine

Human papillomavirus (HPV) infection is a major global cause of cervical and head-and-neck cancers. While the current standard prophylactic approach involves intramuscular (I.M.) vaccination, its requirement for a cold-chain distribution system and skilled healthcare personnel significantly restricts accessibility, especially in resource-limited developing regions. To overcome these limitations, a dissolving microneedle array patch (D-MAP) was designed and developed for HPV vaccine delivery. This innovative approach offers key advantages including cold-chain independence, ease of storage, and potential for self-administration. The oral buccal mucosa was strategically selected as the administration site due to its abundance of antigen-presenting cells (APCs), notably Langerhans cells (LCs), which are crucial for initiating robust immune responses. Through meticulous optimization, a fabrication method for HPV16 virus-like particle (VLPs) within microneedles was successfully established, effectively preserving antigen structural integrity which is pivotal for maintaining immunogenicity. Post-fabrication evaluations confirmed sustained VLP stability and structural integrity for at least six months at ambient temperature. Upon application, HPV16 VLP D-MAP efficiently delivered antigens to the oral buccal mucosa, corresponding draining lymph nodes, and antigen-specific B cells, eliciting robust humoral immune responses which are characterized by germinal center formation, serum-mediated protection, and prolonged immune memory comparable to those achieved in I.M. Gardasil vaccination group. Additionally, this vaccination strategy conferred significant cross-mucosal immunity, providing protection in both buccal and vaginal mucosa, the primary sites of HPV infection. These findings demonstrate the feasibility and efficacy of VLP microneedle-based buccal vaccination, highlighting its potential as an accessible and effective alternative to conventional HPV vaccines.

Key words : HPV, microneedle, vaccine, mucosal immunity, humoral immunity

1. Introduction

Human papillomavirus (HPV) is the most common sexually transmitted virus, with approximately 13 millions new diagnoses occurring and over 400,000 deaths attributed to HPV-mediated cancer annually[1, 2]. Of more than 200 identified HPV subtypes, high-risk types such as HPV16 and HPV18 are strongly associated with cervical and oropharyngeal cancers[3]. The virus is primarily transmitted through sexual contact, but skin-to-skin and vertical transmission from mother to child has been documented in several studies[4]. Historically, HPV has been primarily regarded as a female-centered virus due to its strong association with cervical cancer which ranks the 4th most common cancer among global female populations and primary contributor of the HPV-related cancer burden. Consequently, early public health campaigns mainly targeted adolescent girls for vaccination[5].

However, emerging evidence revealed that HPV affects a broader population, contributing to oropharyngeal, anal, and penile cancers in men, infecting individuals across diverse age and genders. Furthermore, lifestyle habits such as smoking and alcohol consumption are known to accelerate the progression of HPV-mediated cancers[6]. This shift in understanding has led to increased emphasis on gender-neutral vaccination strategy. Implementation of gender-neutral vaccination routine has reduced HPV-related cancer occurrence in United States[7] and significant reduce of HPV infection rate and enhanced herd immunity in Finland[8].

One of the major challenges of HPV control lies in its clinical latency. Infections are often asymptomatic and may remain undetected for extended periods, ranging from weeks to months[9, 10]. Consequently, many individuals become aware of the infection often at advanced disease stages[11]. With no available antiviral treatment for HPV, prophylactic vaccination is a sole effective and preventive measure. Gardasil and Cervarix vaccines are commercially available HPV vaccines[12] which have significantly reduced HPV-related

cancer incidence with national immunization programs[13,14], underscoring the importance of vaccination in HPV control.

Despite their efficacy, conventional vaccine system present several limitations. Traditional vaccines often rely on protein-based vaccines, which require cold-chain storage for antigen stability[15] and trained healthcare personnels for administration[16] which are particularly in resource-limited settings. These factors drive up the overall cost and accessibility to vaccination[17,18]. Furthermore, intramuscular (IM) administration is dependent on systemic IgG responses but fails to elicit mucosal immunity. Induction of mucosal immunity is potent strategy for HPV vaccination as HPV primarily infects the oral and genital mucosa[5]. Previous studies have shown that vaginal mucosa vaccination in animal models elicit robust mucosal IgA responses and generate HPV-specific neutralizing antibodies[19, 20]. Immunization at the site of viral entry or lesion development has been proposed as a logical approach to enhance protection[21].

To overcome the limitations of conventional vaccine system, microneedle (MN) technology has emerged as a promising alternative[22, 23]. MNs, consist of micro-scale needle arrays, are capable of delivering pharmaceutical agents by direct penetration to the site of application[24]. MNs are categorized into four main types based on their structural and functional properties: solid, coated, dissolving and hollow. Among these, dissolving MNs are especially suitable for vaccine delivery due to their ability to encapsulate high payloads of antigens and adjuvants[25]. Also, their use of biocompatible materials such as polymers and sugars left no biohazardous wastes after application[26, 27]. Dissolving MN offer additional advantages including cold-chain independence[28], self-administration potential[29] and pain-free nature which improves patient compliance[30]. Several studies have demonstrated the potential of dissolving MNs for mucosal vaccination. For instance, administration of SARS-CoV-2 dissolving MN vaccine via sublingual tissue induced mucosal immunity[31]. Also, dissolving MN-based respiratory syncytial virus fusion protein

VLPs generated high IgA titer, indicating generation of mucosal immune response[32].

The oral mucosa is an attractive target for mucosal vaccination due to its low enzyme activity which minimizes antigen degradation[33] and abundance of antigen presenting cells (APCs) such as dendritic cells (DCs) and Langerhans cells (LCs) which aids enhanced antigen uptake and delivery[33, 34]. Unlike other mucosal tissues such as sublingual and gingiva, oral mucosa is characterized by its non-keratinized epithelium, allowing undemanding penetration of MNs[35, 36]. Ma and colleagues first testified the feasibility of oral mucosal vaccination using MNs in a rabbit model, showing strong induction of HIV gp140-specific IgA[37].

In this context, this study sought to leverage the cost-effectiveness and adaptability of dissolving MNs for the development of an oral mucosal HPV vaccine. Oral buccal mucosa was strategically selected to promote both systemic and cross-mucosal protection against HPV. Virus-like particles (VLPs) were selected as the vaccine antigen due to their high immunogenicity and stability resistant to the physical stresses during fabrication process. The dissolving microneedle arrayed patch of HPV16 VLP (16V-DMAP) was fabricated based on centrifugal casting method. Penetration and dissolution efficiency of needles, post-fabrication antigen integrity and long-term stability at ambient temperature were evaluated. The immunogenicity and protective efficacy of the 16V-DMAP were evaluated in comparison with conventional IM vaccination of Gardasil in mouse model. To assess the immunogenic potential of this platform, antigen delivery and key immunological parameters such as germinal center (GC) formation, antigen-specific antibody and neutralizing antibody titers were measured. Additionally, protective efficacy was evaluated through *in vivo* HPV pseudovirus challenge. The results demonstrated that 16V-DMAP induced robust humoral immunity, generated antibody responses comparable to those elicited by IM vaccination and conferred effective mucosal protection against HPV pseudovirus infection. These findings support the potential of DMAP-based oral mucosal

vaccine delivery as a practical and innovative strategy for HPV prevention.

2. Materials and Methods

2.1. Animal model

Six-week-old female BALB/c mice were purchased from Orient Bio (Seongnam, South Korea). The animals were maintained under specific pathogen-free (SPF) conditions at Yonsei University College of Medicine. The animal experimental protocols were approved by the Institutional Ethical Committee of Yonsei University College of Medicine. All experiments were performed in accordance with the approved guidelines of the Institutional Ethical Committee.

2.2. Fabrication of HPV16 VLP-DMAP

The dissolving microneedle array patch (DMAP) used in this study was designed, optimized and fabricated by Quad Medicine (Seongnam, South Korea). DMAP was prepared using micro-molding technology. The master of the microneedles is characterized by 21 pyramid-shaped tips on a 3 mm circular base. The tip measurements include a height of 550 μm, a width of 280 μm, a tip-to-tip interval of 580 μm, and a base-to-base interval of 300 μm. Prior to the DMAP preparation, a replica of the mold was created using polydimethylsiloxane (PDMS; SYLGARD 184, Dow Corning). The tip solution was formed of 0.05% (w/v) VLPs, 0.01% (w/v) CTA1, 2.5% (w/v) D-(+)-Trehalose dihydrate (Sigma Aldrich, St. Louis, MO, USA), and 1.62% (w/v) carboxymethyl cellulose sodium salt (low viscosity CMC, Sigma Aldrich). The DMAP base gel was prepared by adding 20% CMC to distilled water (w/v). Approximately 20 μL of the tip solution was then poured into the PDMS mold. To fill the mold's cavities, a centrifuge was utilized, operating at a force of 5,000 x g for 1 hour. Finally, 30 mg of the microneedle base gel was loaded into the mold and centrifuged overnight at a force of 5,000 x g, ensuring complete drying. A Scanning Electron Microscopy (SEM) JSM-7500F (JEOL, Tokyo, Japan) was used to image the master of the microneedle. The image of the D-MAP was inspected using a Leica M205C microscope with FusionOptics (Leica, Wetzlar, Germany).

2.3. Immunization

Immunization groups were divided into four groups: (1) intramuscular (I.M.) PBS, (2) I.M. Gardasil-4 (MSD, Seoul, South Korea), (3) Mock-microneedle (MN), and (4) HPV16-VLP DMAP. For I.M. groups, sterile 1X phosphate-buffered saline (PBS) (Invitrogen™, Massachusetts, United States) or 1/10th of the human dose of Gardasil-4 was injected into the right hind limb of mice. For oral mucosa administration, mice were anesthetized, and Mock-MN and HPV16-VLP DMAP were applied to the left oral buccal mucosa for 20 minutes to ensure complete dissolution.

2.4. Flow cytometry analysis

Mice were euthanized in CO_2 chambers prior to organ collection. Cervical draining lymph nodes were surgically harvested and placed in FACS buffer (0.5% BSA/PBS). Single cell suspensions were prepared by mechanical dissociation and red blood cells were lysed using ACK lysis buffer (Biosesang, Yongin, South Korea). Cells were prepared in FACS buffer and Fc Receptors were blocked using purified anti-mouse CD16/32 (BioLegend, San Diego, California, USA) for 10 minutes. Lymph node cells were stained with diluted antibodies: LIVE/DEAD™ Fixable Near-IR Dead Cell Stain Kit (Invitrogen ™, Waltham, Massachusetts, USA), anti-mouse CD19, anti-mouse B220, anti-mouse CD95, anti-mouse GL-7, anti-mouse CXCR5, anti-mouse PD-1 (BioLegend, San Diego, California, USA) for 20 minutes on ice. Samples were washed twice with FACS buffer and analyzed using BD celesta™ Cell Analyzer (BD Biosciences, New Jersey, USA). Data were further processed and analyzed using FlowJo software.

2.5. Tissue immunofluorescence imaging

Cervical lymph nodes were surgically isolated and embedded in Tissue-Tek ® Cryo-Mold and Tissue-Tek® O.C.T Compound (Sakura Finetek USA, Torrance, California, USA), and stored at -80°C. Tissues were sliced into 5μm thickness by HM525 cryostat

(Thermo Scientific, Waltham, Massachusetts, USA). Tissue sections were dehydrated using -20°C chilled acetone for 2 minutes and rinsed with PBST (0.05% Tween 20 in 1X PBS). Blocking was performed for 30 minutes at room temperature using 10% goat serum (Thermo Scientific, Waltham, Massachusetts, USA) prepared in PBS. Tissues were stained with anti-mouse B220, anti-mouse TCR-β, anti-mouse GL-7 (BioLegend, San Diego, California, USA) for 2 hours at room temperature. Stained sections were mounted with ProLong™ Gold Antifade (Invitrogen, Waltham, Massachusetts, USA). Images were acquired with THUNDER Imaging Systems (Leica, Wetzlar, Germany). Raw images were processed using Fiji/ImageJ. Germinal center (GC) follicles were quantified by identifying $GL7^+$ follicles, which were selected using "Magic Wand" function on a threshold binary image via Fiji/ImageJ.

2.6. HPV16 pseudovirus production

Schematic procedures of HPV16 pseudovirus production are briefly described in Figure 4A. HEK293TT cells were seeded on 175T flask (SPL, Pocehon-si, South Korea) at a density of 1.3 x 10^7 cells per flask a day prior to transfection. The following day, when the cells reached 80% confluency, cells were co-transfected with 39μg p16SheLL plasmid (Addgene, Watertown, MA, USA) and luciferase reporter plasmid using Turbofect™ transfection reagent (ThermoFihser, Massachusettes, USA) and Opti-MEM™ Reduced Serum Medium (ThermoFisher Scientific, Massachusettes, USA). Cells were incubated at 37°C 5% CO_2 incubator for 48 hours. Cells were washed with 1X PBS (Invitrogen™, Massachusetts, USA), detached by 0.05% trypsin-EDTA (HyClone, Marlborough, USA) and neutralized with Dulbecco's Modified Eagle Medium (DMEM) (Cytiva, Marlborough, USA). Cells were collected in 50mL conical tubes (SPL, Pocheon-si, Gyeonggi-do, South Korea), centrifuged at 300 x *g* for 10 minutes. Supernatants were discarded and cell pellets were resuspended with sterile DPBS, transferred to siliconized microcentrifuge tubes, and centrifuged at 300 x *g* for 10 minutes. Collected cell pellet were resuspended in lysis buffer (DPBS with 1% of Brij58, 0.2% of RNase cocktail) and incubated at 37°C water bath

overnight to allow capsid maturation. The next day, lysates were incubated on ice for 10 minutes, spin down at 10,000 x *g* for 10 minutes at 4°C. The supernatants were collected, remaining cell pellets were resuspended with DPBS and centrifuged again. This process was repeated twice. Pooled lysates were purified using iodixanol gradient ultracentrifugation. OptiPrep™ (Sigma-Aldrich, Missouri, USA) were diluted in 0.8M NaCl-DPBS to make 39%, 33%, 27% OptiPrep™ solutions. Each 3 mL layer was sequentially layered into 13.2 mL Open-Top Thinwall Ultra-Clear tubes (Beckman, California, USA) from highest to lowest density. The collected lysate supernatants were carefully layered on top and ultracentrifugation was performed using an XL-100K ultracentrifuge (Beckman, California, USA) at 280,000 x *g* for 16 hours at 16°C. After 16 hours, pseudovirus-containing fractions were collected using a 1mL pipette (Eppendorf, Hamburg, Germany). Each fraction was analyzed by 10% Sodium dodecyl sulfate polyacrylamide gel electrophoresis (SDS-PAGE) followed by coomassie blue staining to detect and quantify the HPV16 L1 capsid protein (Figure 4B).

2.7. HPV16 pseudovirus infectivity test

HEK293TT cells were seeded with 3 x 10^4 cells/well confluency on 96-well flat-bottomed plate (SPL, Pocheon-si, Gyeonggi-do, South Korea) and incubated for 4-6 hours at 37°C, 5% CO_2 incubator (ThermoFisher, Massachusetts, USA). Each fraction of HPV pseudovirus were diluted in DMEM 10-fold 3-point serial dilution. Diluted pseudovirus were treated to 293TT plated plate, incubated for 72 hours and luciferase activity was measured by ONE-Glo™ Luciferase assay system.

2.8. HPV16-specific enzyme-linked immunosorbent assay (ELISA)

96 Well EIA/RIA Plate (Corning, Glendale, Arizona, USA) was coated with 25ng of HPV16 L1 VLP per well and incubated overnight at 4°C. Plates were washed and blocked by 1% BSA/PBS for 2 hours at 37°C incubator. Blood of immunized mice were obtained by retro-orbital bleeding. Blood samples were centrifuged, and sera was aliquoted and

preserved in -80°C deep freezer until the assay. Serum was serially diluted 4-fold with 8 points in 1%BSA/PBS. Diluted serums were treated to antigen coated plate and incubated at 37°C for 2 hours. Goat Anti-Rabbit IgG, IgM, IgA-HRP (SouthernBiotech, Birmingham, Alabama, USA) antibodies were diluted in PBST(0.05% Tween-20 in PBS), treated to each well and incubated overnight at 4°C. Detection of antigen-specific serum was performed using GloMax® (Promega Korea) with 450 nm of absorbance after treating SureBlue™ TMB 1-Component Microwell Peroxidase Substrate (SeraCare, Millford, Massachusetts, USA) and stopping buffer 1mol/L sulfuric acid solution (SAMCHUN, Gangnam, South Korea).

2.9. Neutralization assay

HEK293TT cells were seeded on 96 Well Cell Culture Plate (NEST, Jiangsu, China) 5 hours prior to the assay with $3x10^4$ density per well and incubated at 37°C. Serum samples were acquired as mentioned in method of enzyme-linked immunosorbent assay. Serum was thawed prior to use and diluted in HyClone Dulbecco's Modified Eagle Medium (DMEM) with high glucose (Cytiva, Marlborough, USA) with 4 point 8-fold serial dilution. HPV16 pseudovirus was added to the mixture and incubated in a 4°C cold room for 1 hour on a rock shaker, then treated to a cell-seeded plate and incubated for 72 hours. 100μL of culture medium was discarded and 100μL of ⅓ diluted ONE-Glo luciferase assay reagents (Promega, Madison, Wisconsin, USA) were added to each well, incubated on a rock shaker for 3 minutes, and resuspended thoroughly. 150 μL of lysates were transferred to 96-well flat bottomed black plate for luminescence measure. The luminescence was measured using a Glomax microplate reader (Promega, Wisconsin, United States).

2.10. Enzyme-linked immunosorbent spot (ELISpot)

The membrane of 96-well nitrocellulose-backed microplates (Milipore, Massachusetts, USA) were activated by treating 70% EtOH, then washed with 1X PBS 3 times. HPV16 L1 VLP were diluted with 5ug/mL concentration and coated on plate for overnight at 4°C. Antigen-coated plates were washed with 1X PBS for 5 times, blocked with complete RPMI (Cytiva, Marlborough, USA) supplemented with 10% FBS (Cytiva, Marlborough, USA) for 2 hours at 37°C 5% Co_2 incubator. Blocking media were discarded, washed 3 times with PBS, bone marrow cells with $1x10^6$ density were treated to plates and incubated for 4 hours at 37°C Co_2 incubator. Plates were washed for 5 times with 0.05% PBS-T(0.05% Tween-20 in 1X PBS), and goat anti-Rabbit IgG, IgM, IgA-HRP (SouthernBiotech, Birmingham, Alabama, USA) antibodies were diluted in 0.05% PBST treated to each well and incubated overnight at 4°C. Plates were washed with 1X PBS for 5 times, AEC substrate (BD Biosciences, New Jersey, USA) were treated for 20 minutes until the spot color develops and washed with distilled water, placed in the dark place upside down to dry the plate. Spot was quantified by ImmunoSpot (CTL, Cleveland, USA).

2.11. *In vivo* pseudovirus challenge

BALB/c mice were subcutaneously injected with 3 mg of Depo-Provera (medroxyprogesterone acetate, Pfizer, New York, USA). Three days later, mice were anesthetized, and the oral and vaginal mucosa were gently abraded using a needle cartridge and cytobrush, respectively. HPV16 pseudovirus encoding firefly luciferase (HPV16 PsV-FLuc) was mixed with 3% carboxymethyl cellulose (CMC), and 20 μL of the mixture was applied to both the oral and vaginal mucosal surfaces.

2.12. Passive transfer assay

BALB/c mice were subcutaneously injected with 3 mg of Depo-Provera. After 3 days, sera were collected from MN-Mock and 16V-DMAP immunized mice. A total of 100 μL of diluted serum (20 μL of serum mixed with 80 μL of PBS) was administered

intravenously into naive mice. After 24 hours, mice were challenged with HPV16 PsV-FLuc as described in Section 2.11.

2.13. Bioluminescence imaging

Three days after PsV-FLuc inoculation, mice were anesthetized and placed in a supine position within the IVIS Spectrum imaging chamber (Xenogen, Alameda, California, USA). A 20 μL volume of D-Luciferin (7.8 mg/mL; Gold Biotechnology, St. Louis, Missouri, USA) was applied into either the oral or vaginal mucosa using a positive-displacement pipette. Two-dimensional bioluminescence images were acquired within 2 minutes of luciferin application, using a 3-minute exposure time. Bioluminescence signal intensity (total flux, photons/sec) was quantified by drawing regions of interest (ROIs) over the oral (head) or vaginal (groin) area.

2.14. Statistical analysis

Statistical analyses were performed using GraphPad Prism software. Two-tailed unpaired Student's t-tests were used for comparisons between two groups, and one-way or two-way ANOVA was used for comparisons among multiple groups. Data are presented as means ± SEM. Statistical significance is indicated as follows: * $p < 0.05$, ** $p \leq 0.01$, *** $p \leq 0.001$, **** $p \leq 0.0001$, and ns = not significant ($p > 0.05$).

3. Results

3.1. 16V-DMAP demonstrates successful tissue penetration and preserves antigen integrity post-fabrication process

The characteristics and mechanical performance of DMAP manufactured by micro-molding technology were evaluated. The DMAP, composed of 21 tips, was confirmed to have no bending or breaking at the tip ends when observed through a microscope (Figure 1C). In the insertion test on porcine skin, the penetration efficiency was verified (Figure 1D). Among the DMAP formulations set with the ratio of HPV16 L1 VLP and trehalose at 1:0, 1:20, and 1:50, the target antigen content could only be confirmed at a ratio of 1:50 (Figure 1E). After more than 30 minutes after injection into porcine skin, the dissolution kinetics showed that all the tips of DMAP penetrated into the skin (Figure 1F).

The DMAP of the 1:50 VLP to trehalose formulation preserved the content of HPV16 L1 VLP for 7 days under accelerated storage conditions (40±2℃/75±5% RH) (Slope value: -0.051). On the other hand, DMAP without a stabilizer showed a drastic decrease in antigenicity under acceleration conditions (Slope value: -0.55), and the DMAP formulation of 20 times more trehalose also showed a rapid decrease in antigenicity (Slope value: -0.27) (Figure 1G). It was confirmed by DLS and TEM that there is no aggregation of VLP in the DMAP manufactured with a VLP to trehalose ratio of 1:50 (Figure 1H-I). In the DLS analysis, the number-based distribution of VLP before and after DMAP production was consistent, with measurements of 51.17±7.72 nm (PDI: 0.27±0.02) and 54.33±8.33 nm (PDI: 0.32±0.01) respectively. The antigenicity of the DMAP, composed of a 1:50 VLP to trehalose formulation, has been confirmed to remain stable for 6 months under both refrigeration (5±3℃) and room temperature (25±2℃/60±5% RH). Importantly, the stability is expected to last up to 6 months as the slope value is close to 0 at both refrigeration (-1.96) and room temperature (1.7) (Figure 1J-K).

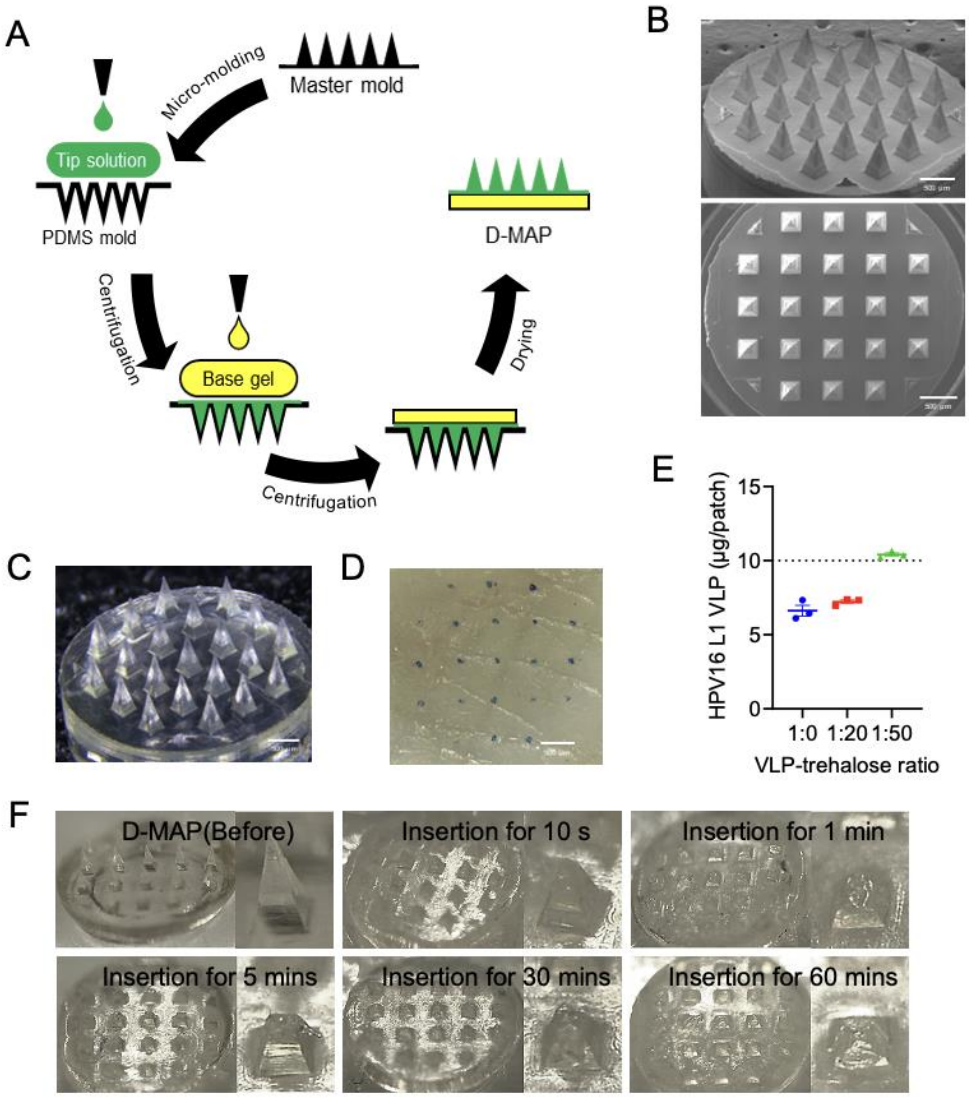

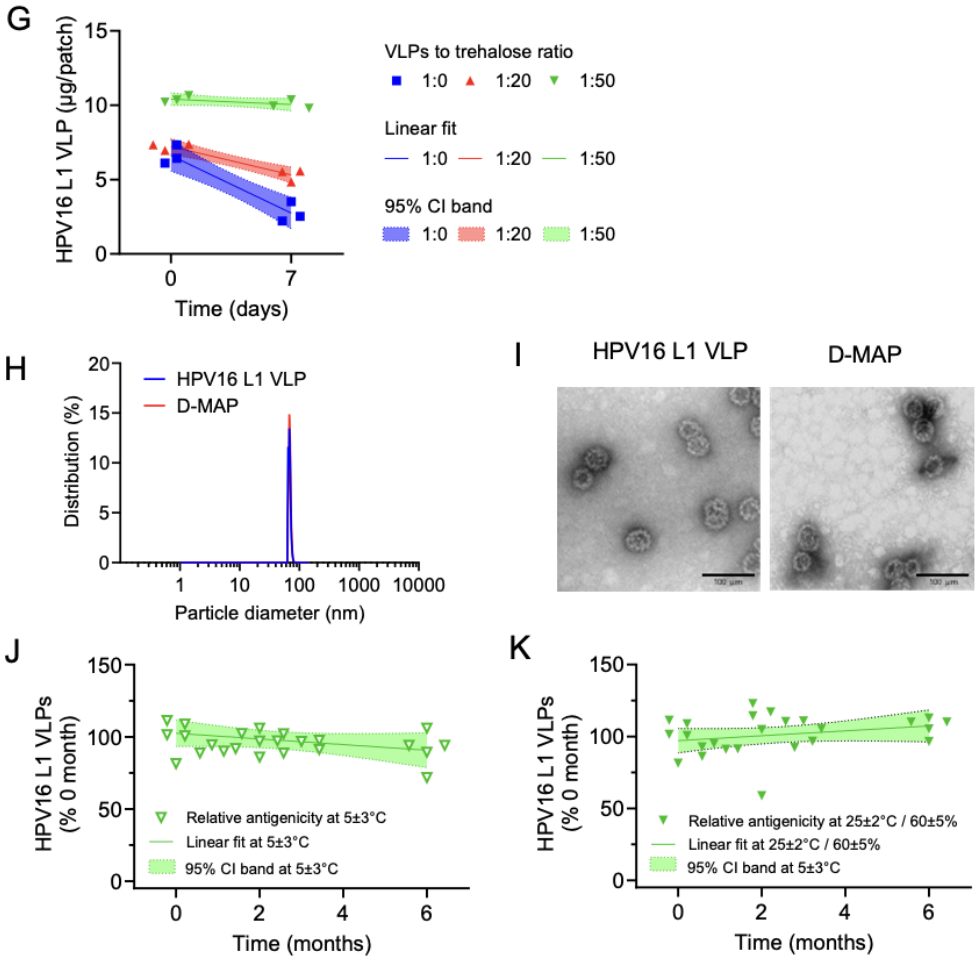

Figure 1. Fabrication and stability evaluation of a DMAP . (A) A schematic diagram of DMAP. (B) A SEM image of the microneedle master. (C) A microscopic image of DMAP. (D) The penetration efficiency of D-MAP on porcine skin. (E) The HPV16 L1 VLP concentration in DMAP. (F) The dissolution kinetics of DMAP before and after insertion into porcine skin at intervals of 10 seconds, 1, 15, 30, and 60 minutes. (G) Evaluation of the accelerated stability of HPV16 L1 VLP based on the trehalose ratio in DMAP. Comparative analysis of HPV16 L1 VLP by (H) DLS and (I) TEM, before and after DMAP production. Long-term stability evaluation of D-MAP, composed of a 1:50 mixture of VLP

and trehalose, at (J) refrigeration (5±3℃) and (K) room temperature (25±2℃/60±5% RH).

3.2. 16V-DMAP efficiently delivered antigens to the oral mucosa, draining lymph nodes, and ultimately to antigen-specific B cells

Antigens are key molecules that interact with lymphocytes and initiate immune responses[38]. However, components such as saliva and enzymes may hinder antigen retention and delivery to the draining lymph nodes (drLNs)[39, 40] when vaccines are administered via oral mucosa. To assess whether antigen integrity is preserved following 16V-DMAP administration, AF647-labeled 16V-DMAP and mock MNs (MN-Mock, without antigen) were applied to the right oral buccal mucosa of anesthetized mice for 20 minutes to allow proper dissolution of needles. Antigen retention was monitored 1-hour post-administration using an *in vivo* imaging system (IVIS). Fluorescent signals from AF647 were observed at the application site of 16V-DMAP group, indicating localized antigen retention on oral buccal mucosa (Figure 2A-B). To examine antigen drainage to adjacent lymph nodes, cervical drLNs were surgically excised 24 hours post-immunization. Fluorescence was still detectable in drLNs of 16V-DMAP group, suggesting successful intact antigen delivery from the administration site to the LNs without degradation (Figure 2C-D). These results confirm that oral buccal mucosa immunization with 16V-DMAP enables safe and targeted transport of antigens to the site of administration and secondary lymphoid organ (SLO), a critical site for activation of humoral immune response[41]. Given that direct activation of naïve B cells in SLO is a critical prerequisite for the initiation of germinal center (GC) reactions[42], B cell engagement with delivered antigens from cervical drLNs were analyzed by flow cytometry analysis. As expected, a distinct population of antigen-specific B cells (AF647+ B220+) was observed in the 16V-DMAP group, whereas the MN-Mock group showed no presence of activated B cells (Figure 2E-F). In summary, oral buccal administration of 16V-DMAP enabled intact antigen delivery to both injection site and drLNs, effectively promoting local B cell activation.

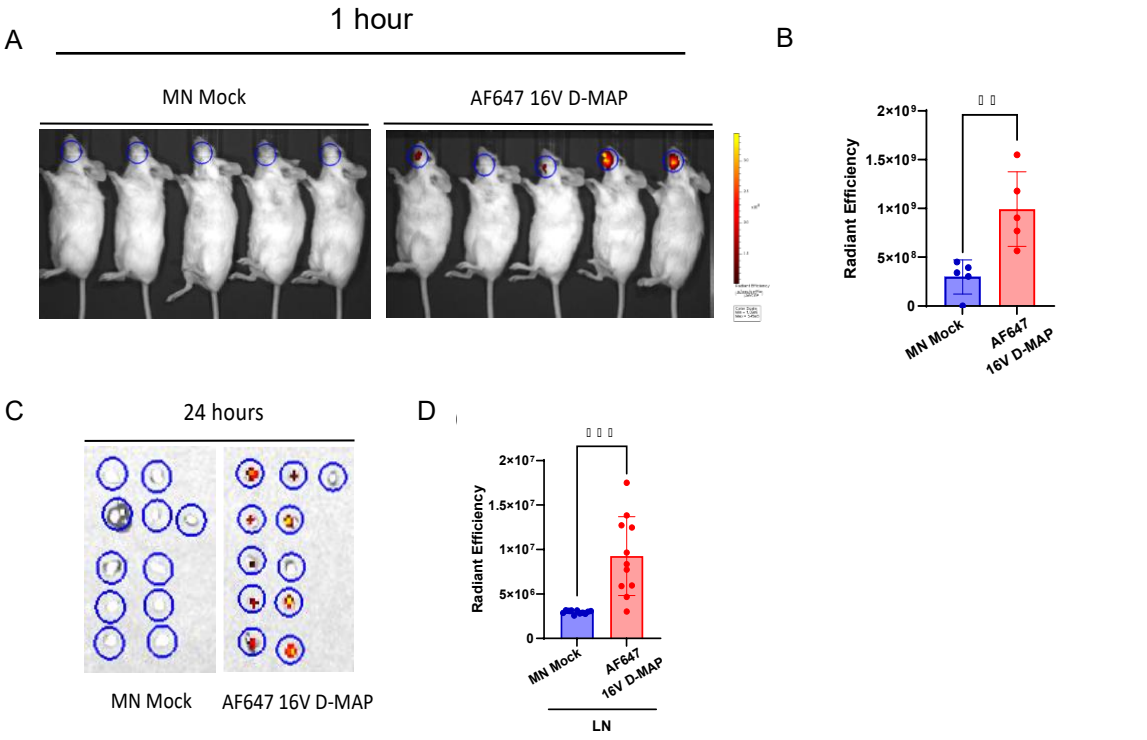

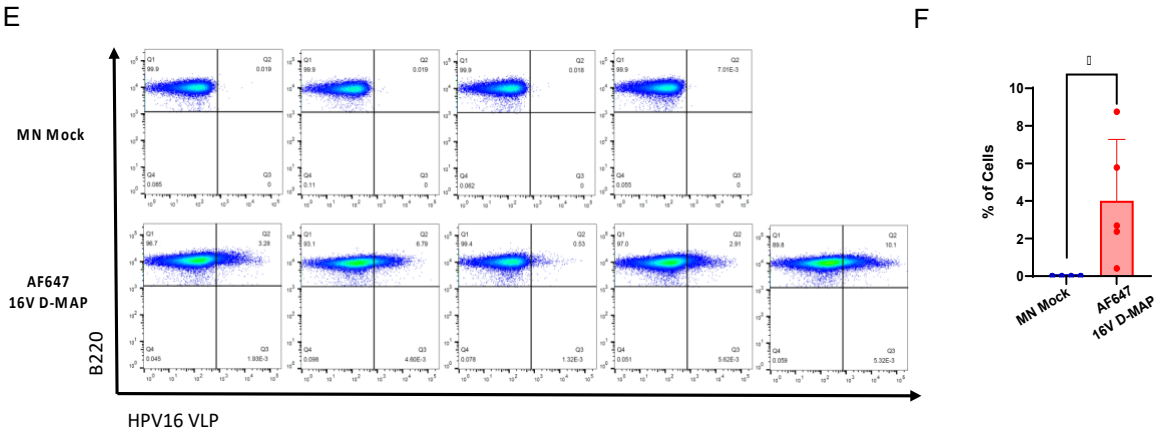

Figure 2. Evaluation of antigen delivery to immunization site and adjacent drLN following 16V-DMAP immunization. (A) Representative image of IVIS imaging of mice 1 hour after application of MN-Mock and AF647-labeled 16V-DMAP on the oral buccal mucosa. (B) Statistic analysis of fluorescence intensity at the application site. (C) *Ex vivo* IVIS imaging of cervical drLNs excised 24 hours post-administration from MN-Mock and AF647-16V DMAP groups. (D) Statistic analysis of fluorescence intensity of excised drLNs. (E) Representative gating plot of HPV16 VLP-specific B cells ($B220^+$ $AF647^+$) in drLNs. (F) Statistical analysis of HPV16 VLP-specific B cells in cervical drLNs. Data are presented as means ± SEM. ns> 0.05, * P<0.05, ** P ≤ 0.01, and **** P ≤ 0.0001 (unpaired t test).

3.3. 16V-DMAP immunization induces robust humoral immunity through enhanced GC response

GC formation is a key indicator of a successful humoral immune response. GC B cells and follicular helper T (T_{FH}) cells are critical participants of this reaction. GC B cells are activated naïve B cells that enter GC and go through somatic hypermutation (SHM), affinity maturation for high-affinity clone selection, and class-switch recombination (CSR), a process which diversifies antibody isotypes and consequently led to differentiation of memory B cells (MBCs) and plasma cells (PCs)[43]. These sequential events require guidance from T_{FH} cells, a specialized subset of $CD4^+$ T cells residing in GC light zone. T_{FH} cells support B cell maturation through cytokine secretion and CD40L-CD40 interactions[44].

To evaluate the quality of humoral immune response elicited by 16V-DMAP immunization, mice were immunized with PBS or Gardasil via intramuscular (IM) injection, and with MN-Mock or 16V-DMAP via oral buccal mucosa. All groups received three doses at two-week intervals. Cervical drLNs were collected after 1st and 3rd boost immunization for flow cytometry analysis of GC B cells and T_{FH} cells (Figure 3A). After the 1st immunization, a notable percentage of GC B cells was observed in the 16V-DMAP group, with frequencies comparable to those of IM-Gardasil group. In contrast, percentage of T_{FH} cells remained modest across all four groups (Figure 3B-C). Followed by 3rd immunization, both GC B cell and T_{FH} cell populations markedly increased, indicating robust induction of GC response (Figure 3D,E). Oddly, the percentage of T_{FH} cells were similar between the MN-Mock and 16V-DMAP groups in both 1st and 3rd immunization dose (Figure 3C,E). This phenomenon is presumed to be the result from minor tissue injury caused by MN insertion, which may serve as a trigger for the secretion of proinflammatory cytokines such as IL-6, IL-21, and IL-12. These cytokines are known to promote T_{FH} cell differentiation during inflammation and tissue repair[45, 46]. This

mechanism likely accounts for the T_{FH} cell induction observed in MN-Mock group, despite the absence of antigen.

To further evaluate GC formation, LN tissues from the MN-Mock and 16V-DMAP groups were stained with B220 (B cell marker), TCR- β (T cell marker), and GL-7 (GC follicle marker) to quantify GC follicle generation. There were either no detectable or only minimal presence of GC follicles in prime immunized groups of 16V-DMAP, but significant increase in numbers and follicle size were observed in 3rd immunized group (Figure 3F-G).

These results depict 3rd boost immunization induce a broader immune response, suggesting robust proliferation and active GC dynamics. In conclusion, 16V-DMAP immunization delivery not only increased the numbers of GC B cells and T_{FH} cells, but also promoted the formation of distinct GC follicles in drLNs upon 3rd boost, demonstrating the efficient induction of a potent humoral immune response.

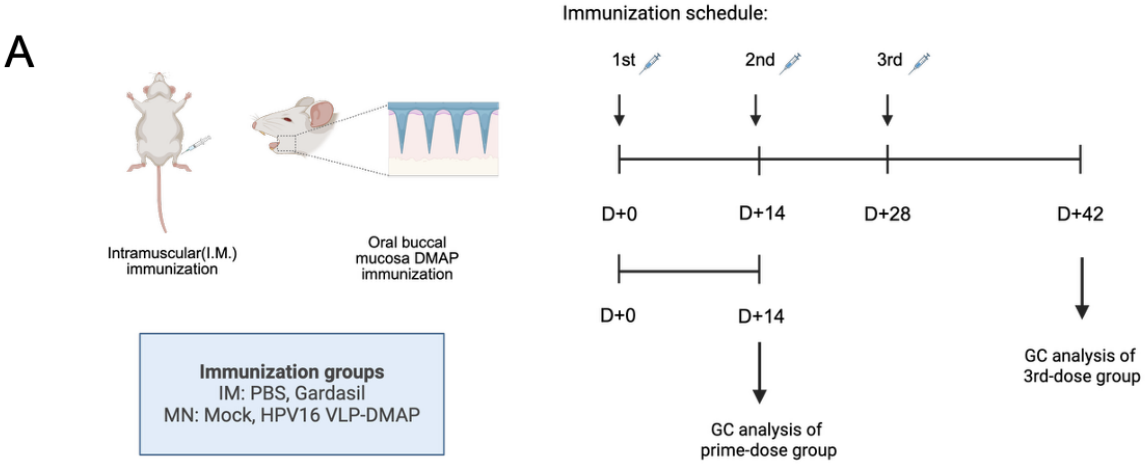

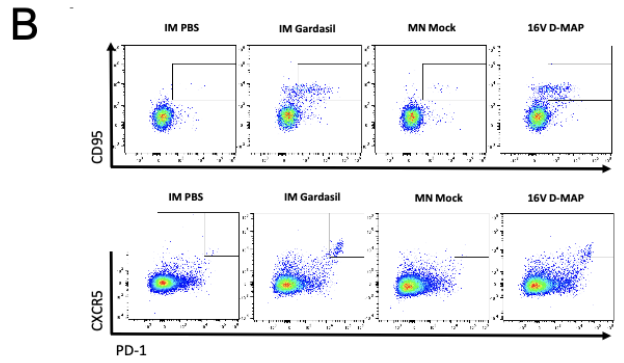

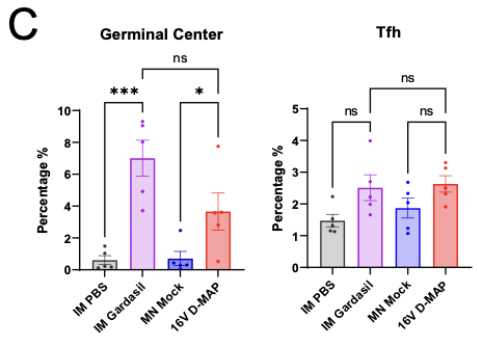

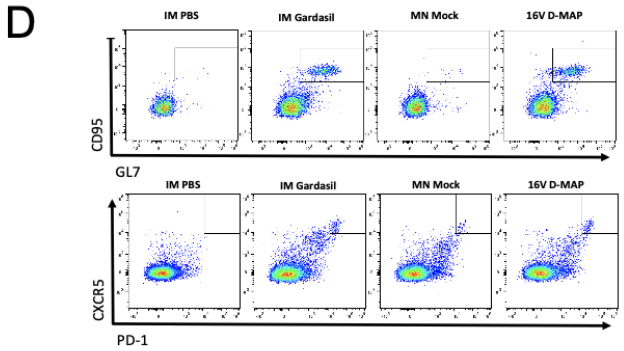

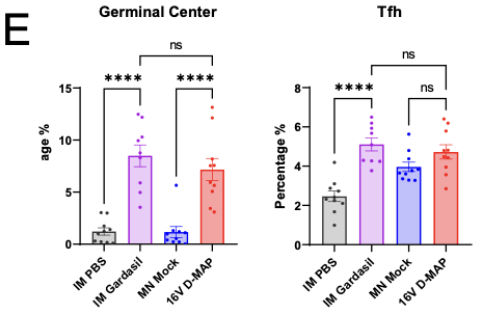

F

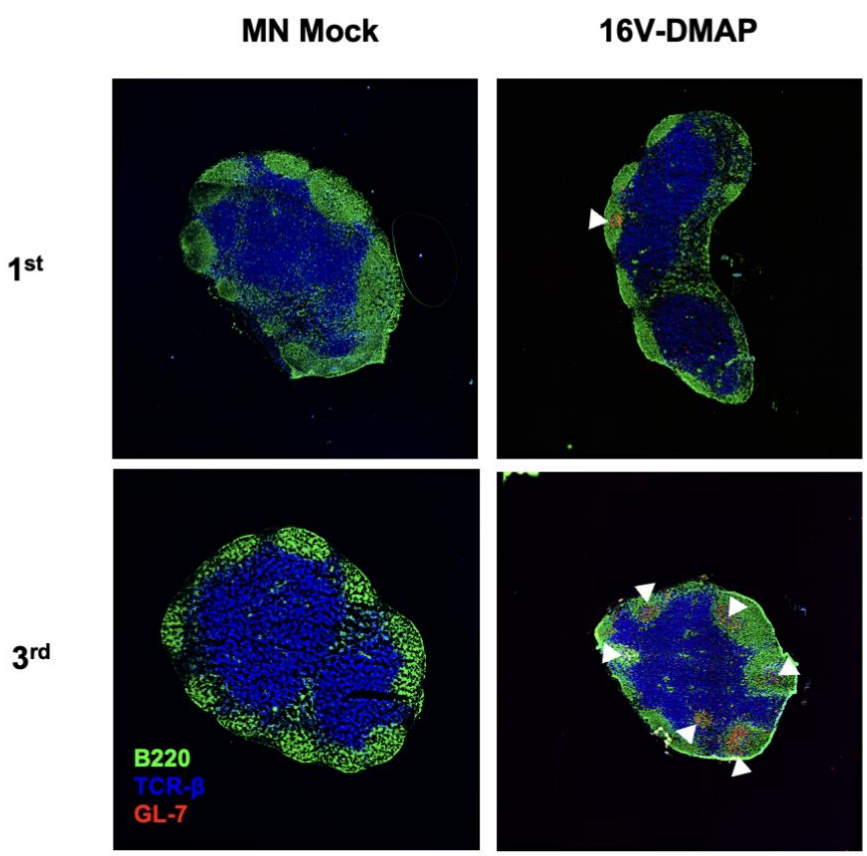

G

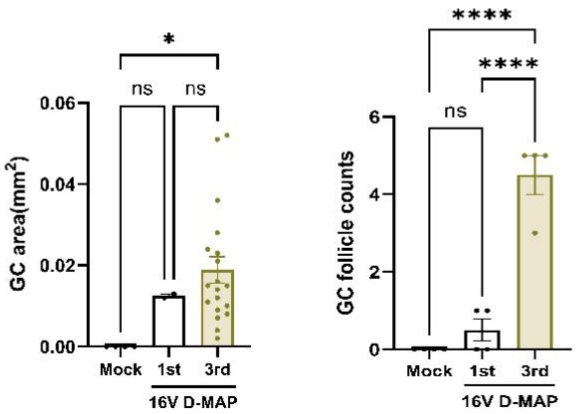

Figure 3. Assessment of GC B cells, T_{FH} cells, and GC follicle structure following 16V-DMAP immunization. (A) Schematic overview of immunization schedule and experimental design. Mice were immunized on days 0, 14, and 28 via IM injection (PBS or Gardasil) or oral buccal administration of MN (Mock or 16V-DMAP). Cervical drLNs were collected on day 14 and 42 for analysis. (B) Representative gating plot of flow cytometry analysis of GC B cells ($CD95^{+}$ $GL\text{-}7^{+}$) and T_{FH} cells ($CXCR5^{hi}$ $PD\text{-}1^{hi}$) in cervical drLNs following the first immunization. (C) Statistical analysis of GC B cells and GC T_{FH} cells in cervical drLNs following the first immunization. (D) Representative gating plot of flow cytometry analysis of GC B cells and T_{FH} cells in cervical drLNs following the 3^{rd} boost immunization. (E) Statistical analysis of GC B cells and GC T_{FH} cells in cervical drLNs following the 3^{rd} boost immunization. (F) Representative image of immunofluorescence staining of cervical drLN sections of 1^{st} and 3^{rd} dose oral buccal mucosa immunized groups stained with B220 (green, B cells), TCR-β (blue, T cells), GL-7 (red, GC follicle). The white triangle marks the location of a GC follicle. (G) Statistical analysis of GC follicle counts and area. Data are presented as means ± SEM. ns> 0.05, * $P<0.05$, ** $P \leq 0.01$, and **** $P \leq 0.0001$ (unpaired t test).

3.4. 16V-DMAP immunization elicits strong and functional antigen-specific humoral immune response.

To evaluate vaccine-induced serum response, HPV16-specific IgM, IgG and IgA titers were measured using enzyme-linked immunosorbent assay (ELISA). As expected, three different isotypes of antibodies were completely undetectable in pre-immune sera (Figure 5B). Following 3rd immunization, a marked increased titer of antigen-specific IgG was detected in both IM-Gardasil and 16V-DMAP groups (Figure 5C). Although this immunization strategy aimed to elicit IgA through mucosal delivery, antigen-specific IgA was barely detectable in the 16V-DMAP group (Figure 5C). Vaginal wash samples were also analyzed for detection of local IgA secretion, but IgA levels in vaginal wash samples remained below the detection threshold (data not shown).

Neutralizing antibodies (NAbs) play a critical role in defense of viral infection by binding to the surface of viral particles and blocking entry into host cells[47, 48]. HPV16 pseudovirus encoding a luciferase reporter plasmid (PsV-FLuc) was produced for assessment of NAbs titer and further *in vivo* experiments. The production and infectivity evaluation of HPV16 PsV-FLuc is described in Figure 4. Titers of NAbs were measured by neutralization assay using HPV16 PsV. Pre-immune sera exhibited negligible neutralizing activity but began to increase after the 1st immunization and reached a 64-fold elevation following the 3rd dose in the 16V-DMAP group, demonstrating efficacious neutralizing capacity comparable to that of the IM-Gardasil group (Figure 5D).

While PCs can appear transiently in the peripheral blood following vaccination or infection, they rapidly undergo apoptosis unless they migrate to the BM[49]. BM serves as a specialized niche that supports the survival of long-lived plasma cells (LLPCs) for extended periods even years and decade. As they are readily maintained in BM, they are essential for continuous antibody production and prolonged immune protection[50, 51, 52]. To evaluate

whether 16V-DMAP immunization successfully induced LLPC maturation to the BM niche, BM-antibody secreting cells (ASCs) were quantified by ELISpot. Antigen-specific IgG-secreting cells were substantially detected in 16V-DMAP group comparable to that of IM-Gardasil, which reflects the result of antigen-specific ELISA (Figure 5C). Surprisingly, serum IgM and IgA were barely detectable in ELISA assessment, but respective ASCs were quantified in 16V-DMAP group (Figure 5F). This discrepancy might be due to the technical limitation of ELISA, which has relatively low sensitivity, whereas ELISPOT offers higher sensitivity for antibody detection[53].

A

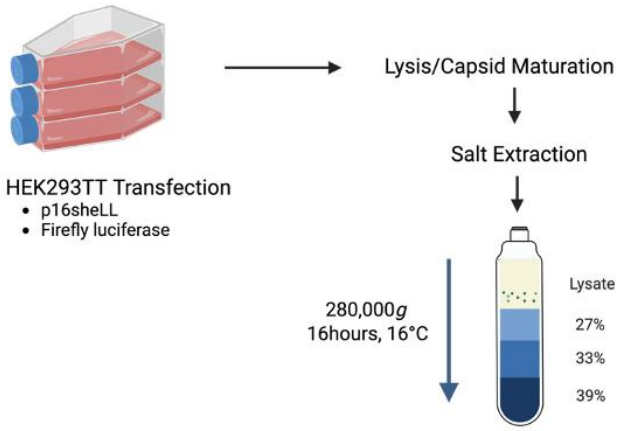

B

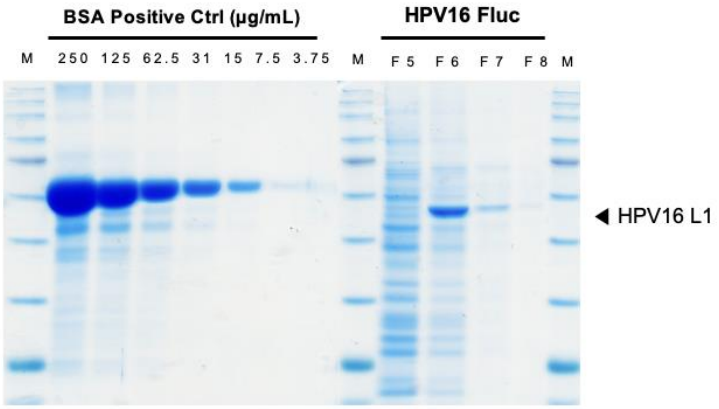

C

	HPV 16				
	F5	F6	F7	F8	N.C
1:100	5.56E+05	1.23E+07	5.51E+06	1.97E+06	1.00E+01
	5.27E+05	1.20E+07	5.50E+06	2.07E+06	4.00E+01
1:1000	7.44E+04	5.49E+06	1.04E+06	2.14E+05	
	8.65E+04	5.66E+06	1.03E+06	2.47E+05	
1:10000	1.42E+04	8.90E+05	9.29E+04	2.20E+04	
	9.16E+03	8.92E+05	1.11E+05	3.06E+04	

Figure 4. Production of HPV16 PsV-FLuc. (A) Schematic overview of HPV16 PsV-FLuc production. HEK293TT were seeded and transfected with HPV16 L1, L2 and luciferase reporter plasmid for 48 hours. Transfected cells were harvested, lysed, and ultracentrifuged with iodixanol density gradient for 16 hours at 280,000 x *g*. (B) Quantification of HPV16 L1 by SDS-PAGE. Bovine serum albumin (BSA) was used as positive control, serially diluted 2-fold 5-point starting from 250ug/mL concentration. HPV16 PsV-FLuc fraction acquired from ultracentrifuge tube were loaded to the SDS-PAGE gel with an order of acquisition. M represents marker, and molecular weight of HPV16 L1 protein is 55kDa. (C) Infectivity test result of harvested HPV16 PsV-FLuc fraction. Each fraction was subjected to a 3-point, 10-fold serial dilution and incubated with HEK293TT cells. After 72 hours of incubation, luciferase activity was measured to assess infectivity.

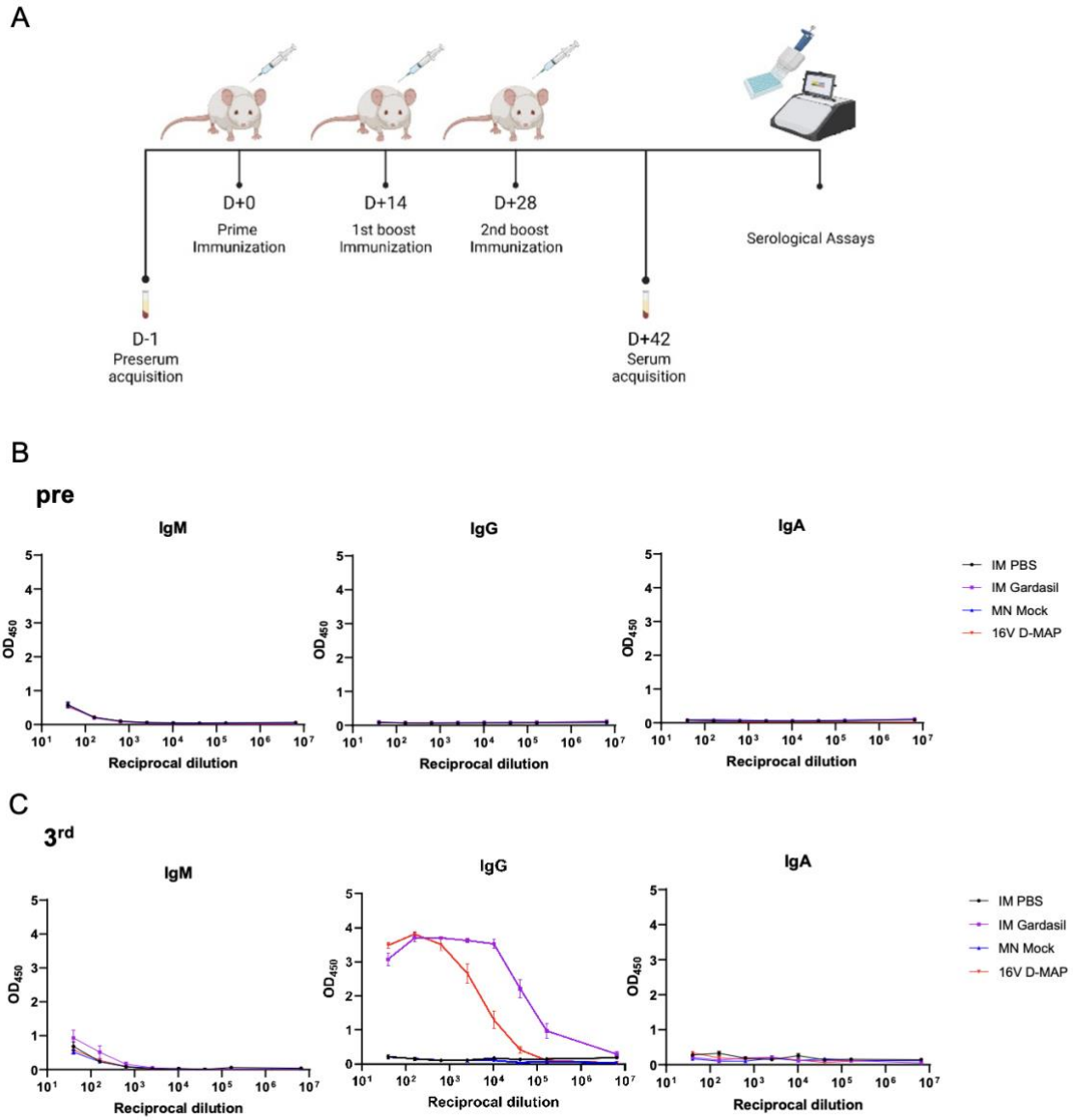

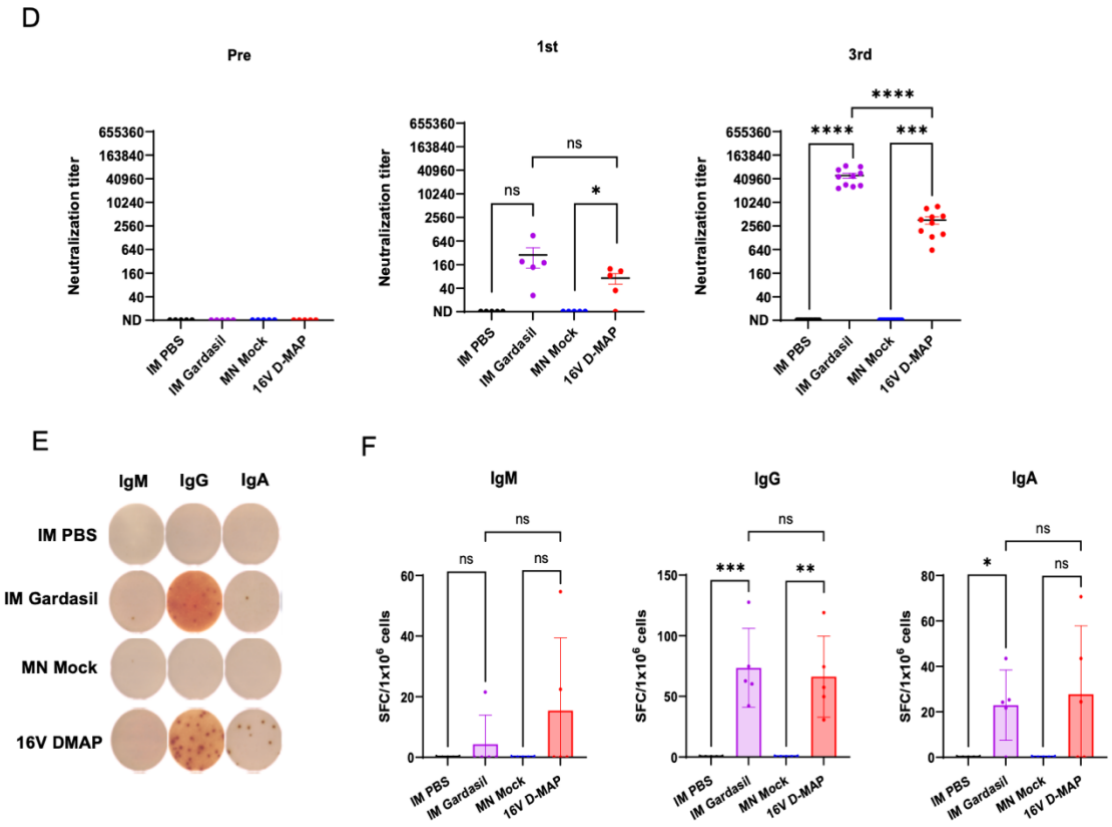

Figure 5. Quantification of antigen-specific immunoglobulins, NAbs, and ASCs following immunization. (A) Schematic overview of immunization schedule and experimental design. Mice were immunized on days 0, 14, 28 via IM (PBS or Gardasil) or MN (Mock or HPV16-VLP DMAP). Serum samples were collected at pre-immunization and two weeks after the 3rd boost immunization. (B) HPV16-specific IgM, IgG, and IgA titers measured by ELISA from pre-immune serum and (C) 3rd immunized serum. (D) NAbs titers against HPV16 pseudovirus in serum collected at pre-immunization, post-1st, and post-3rd immunization time points. (E) Representative ELISpot well images showing HPV16-specific IgM-, IgG-and IgA-secreting plasma cells from BM. (F) Statistical analysis of antigen-specific ASCs per 10^6 BM cells. Data are presented as means ± SEM.

ns> 0.05, * P<0.05, ** P ≤ 0.01, and **** P ≤ 0.0001 (unpaired t test).

3.5. 16V-DMAP immunization confers antibody-mediated protection against HPV16 pseudovirus infection

To evaluate vaccine-mediated protection against infection, PsV-based *in vivo* challenge was conducted. Mice were immunized with three doses of vaccine at two-week interval. Prior to *in vivo* challenge, mice were injected subcutaneously (s.c.) with Depo-Provera, a progesterone hormone that suppresses ovulation and enhances susceptibility to vaginal infection by thinning the epithelium[54]. 3 days later, mice were anesthetized, and the oral and vaginal mucosa were scratched with tattoo needle and cytobrush to mimic microabrasions to ensure viral entry. HPV16 PsV-FLuc diluted in 1.5% carboxymethyl cellulose (CMC) was administered to both abraded tissues. 3 days post-infection, mice were subjected to IVIS imaging to observe pseudoviral activity (Figure 6A). Luciferase signals were clearly detected in oral buccal mucosa of the IM-PBS and MN-Mock groups, indicating active PsV infection. In contrast, no luciferase activity was observed in the IM-Gardasil and 16V-DMAP groups, suggesting these immunized groups successfully mounted protective immunity against HPV16-PsV (Figure 6B-C). Notably, 16V-DMAP immunization provided protection not only at the site of administration but also at the distal vaginal mucosa. This finding implies the induction of cross-mucosal immunity, a phenomenon wherein immune responses generated at one mucosal sites surface disseminate to other anatomically distinct mucosal sites[55].

To determine whether the observed *in vivo* protection is antibody-mediated, a passive transfer experiment was performed. Wild-type BALB/C mice intravenously (i.v.) received 100μL of diluted serum (20μL of serum + 80μL PBS) collected from mice immunized with 3 doses of either MN-Mock or 16V-DMAP (Figure 6D). These mice underwent PsV challenge as previously described. IVIS imaging showed strong luciferase signals in mice that received serum from MN-Mock group. Despite using minimal volume of serum, passive transfer of 16V-DMAP immune serum conferred full protection against PsV

challenge (Figure 6E-F).

These findings demonstrate that oral buccal administration of 16V-DMAP induces functionally protective antibody-mediated immunity against in vivo challenge of HPV PsV and cross-tissue protection at both oral and distal vaginal mucosa.

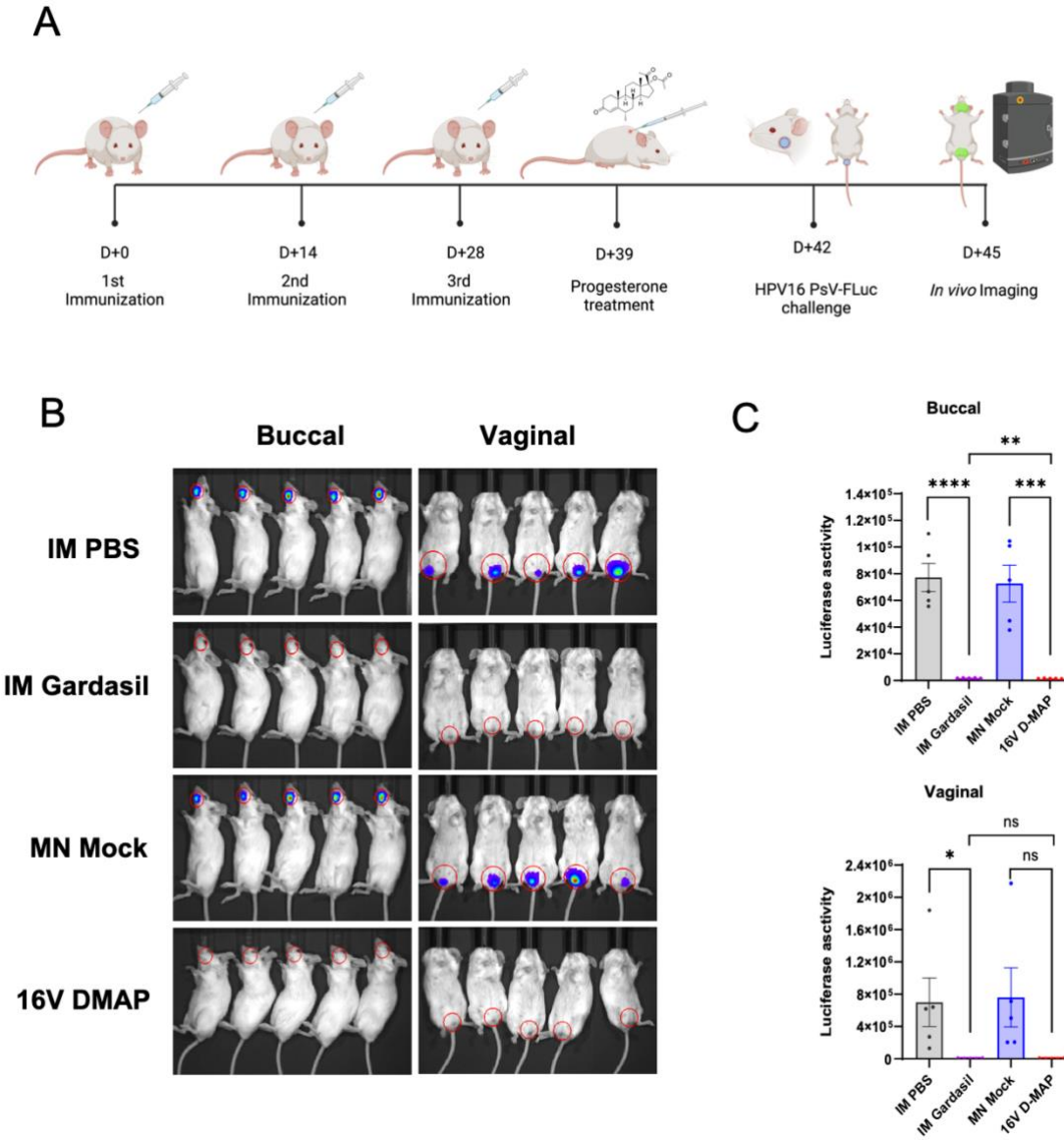

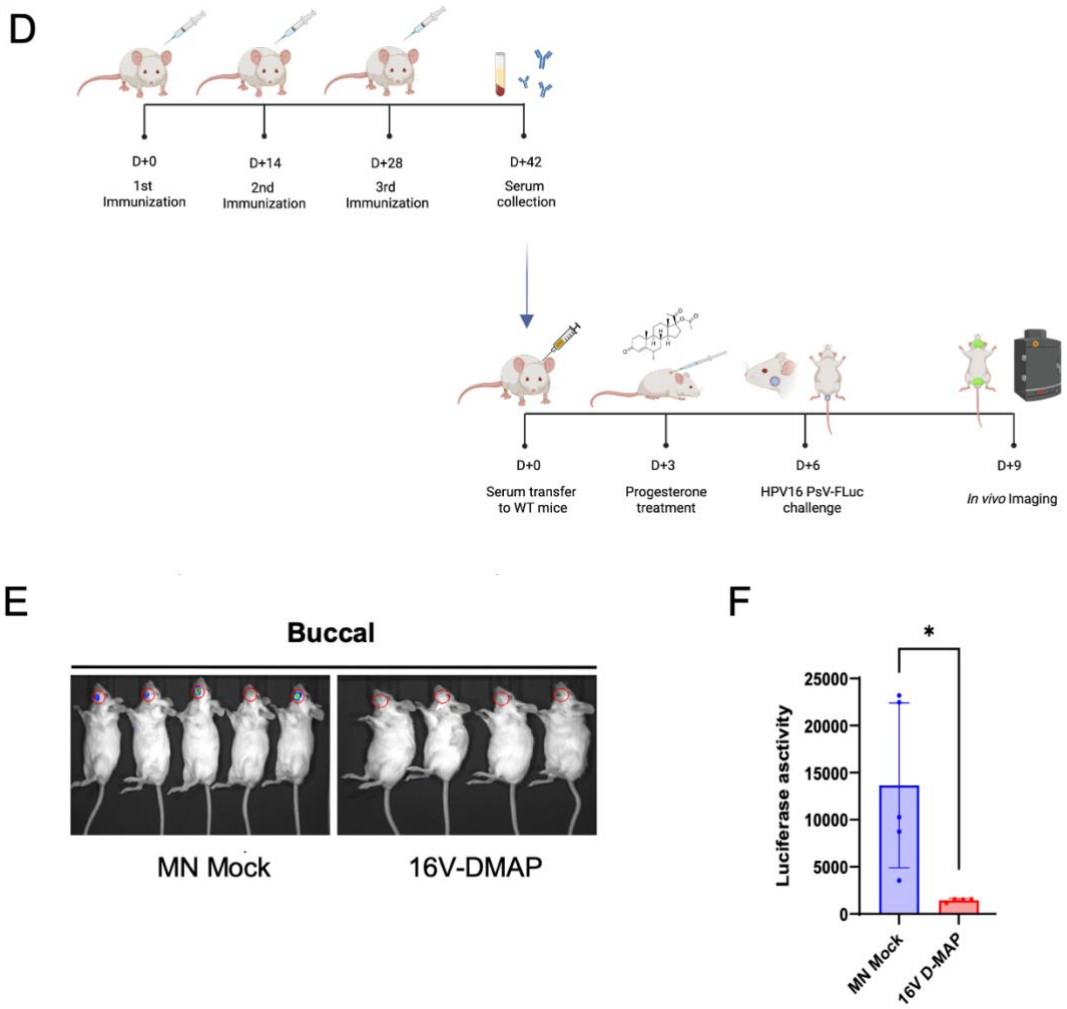

Figure 6. *In vivo* imaging of HPV16 PsV-FLuc infection in actively and passively immunized mice. (A) Schematic overview of immunization schedule and experimental design. Mice were immunized three times via I.M. and MN. HPV16 PsV expressing luciferase were inoculated on oral and vaginal mucosa. Bioluminescence of luciferase activity was measured by IVIS imaging. (B) Representative image of bioluminescence

imaging of oral and vaginal mucosa areas of challenged mice (C) Statistical analysis of luciferase activity of oral and vaginal mucosa tissue. (D) Schematic overview of passive transfer assay. Wild-type BALB/C mice received 100uL of serum of MN-Mock or 16V-DMAP immunized mice. (E) Representative image of bioluminescence imaging of oral and vaginal mucosa areas of challenged mice. (F) Statistical analysis of luciferase activity of oral and vaginal mucosa tissue. Data are presented as means ± SEM. ns> 0.05, * P<0.05, ** P $\leq$ 0.01, and **** P $\leq$ 0.0001 (unpaired t test).

3.6. 16V-DMAP immunization establishes sustained long-term antibody maintenance and *in vivo* protection

Effective vaccination is known to extend immune memory for at least 6 months post-final vaccination[56]. To evaluate the long-term durability of vaccine-induced immunity, mice were immunized 3 times at two-week interval. Six months after the final dose, serum and BM samples were collected and analyzed as outlined in Figure 7A. HPV16-specific IgG remained detectable beyond six months post-immunization. Notably, unlike the short-term analysis (Figure 5C), the IgG titer in the 16V-DMAP group was slightly higher than that of the IM-Gardasil group (Figure 7B). In neutralization assay, IM-Gardasil group showed slight decrease in NAbs titer compared to short-term analysis (Figure 5D), but 16V-DMAP maintained relatively stable titer of NAbs (Figure 7C).

To further assess long-term humoral immunity, antigen-specific LLPCs were quantified via ELISpot. LLPCs, which reside in the BM niche, play a central role in maintaining long-term antibody production. Although the molecular mechanisms regulating LLPC longevity remain unclear, BM LLPCs are widely accepted as a key indicator of durable vaccine efficacy. ELISpot analysis showed comparable frequencies of antigen-specific LLPCs in the IM-Gardasil and 16V-DMAP groups, indicating that DMAP immunization successfully induced durable generation of LLPCs (Figure 7E).

Lastly, to validate long-term *in vivo* protection, all immunized groups were challenged with HPV16 PsV-FLuc six months after vaccination. IVIS imaging revealed no detectable luciferase activity in the oral buccal and vaginal mucosa of both IM-Gardasil and 16V-DMAP groups, indicating vaccine-induced protection persisted for at least 6 months post-immunization (Figure 7F–G). Collectively, these findings demonstrate that 16V-DMAP immunization elicited long-lasting serological and cellular immunity, ultimately conferring effective *in vivo* protection.

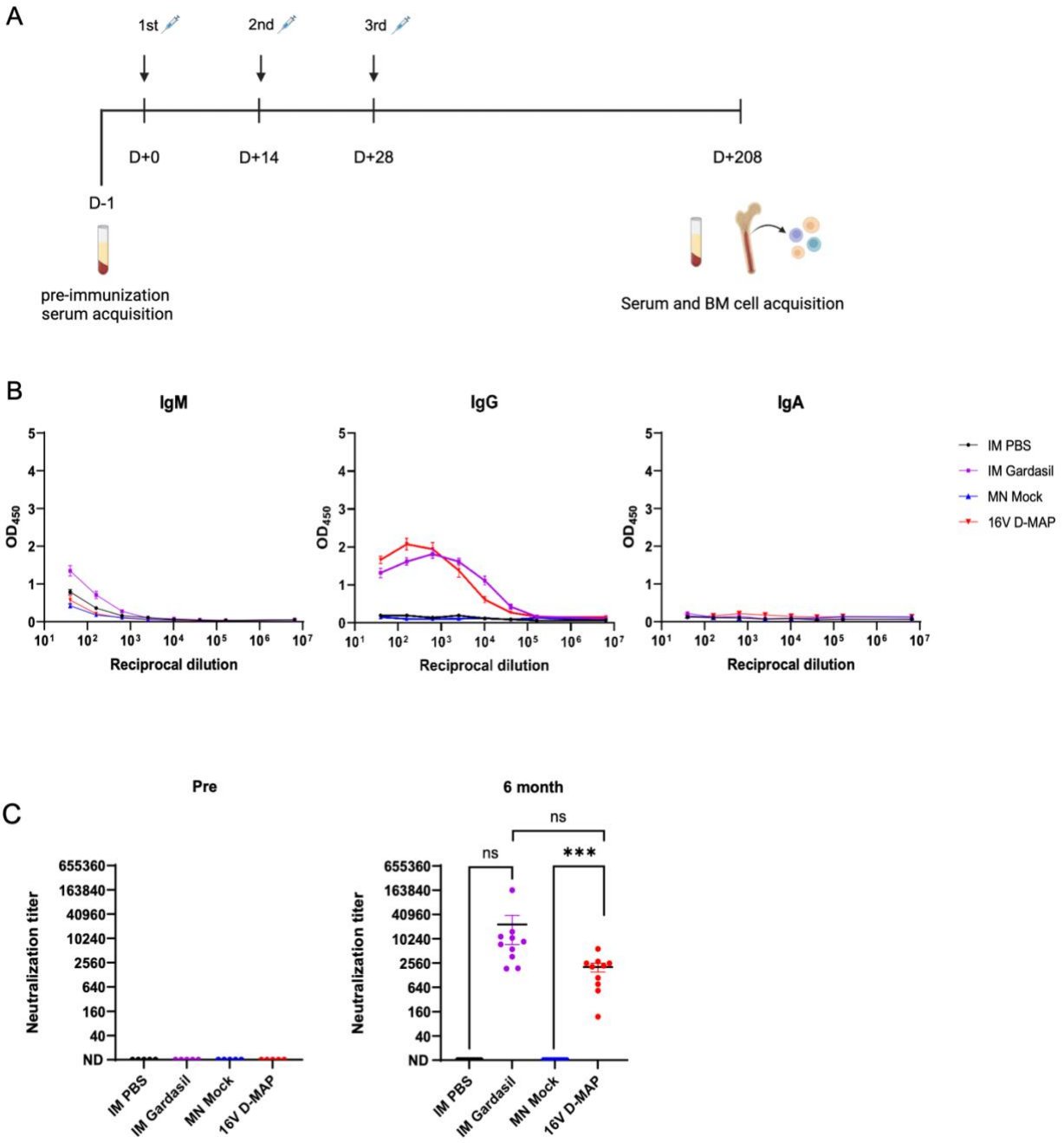

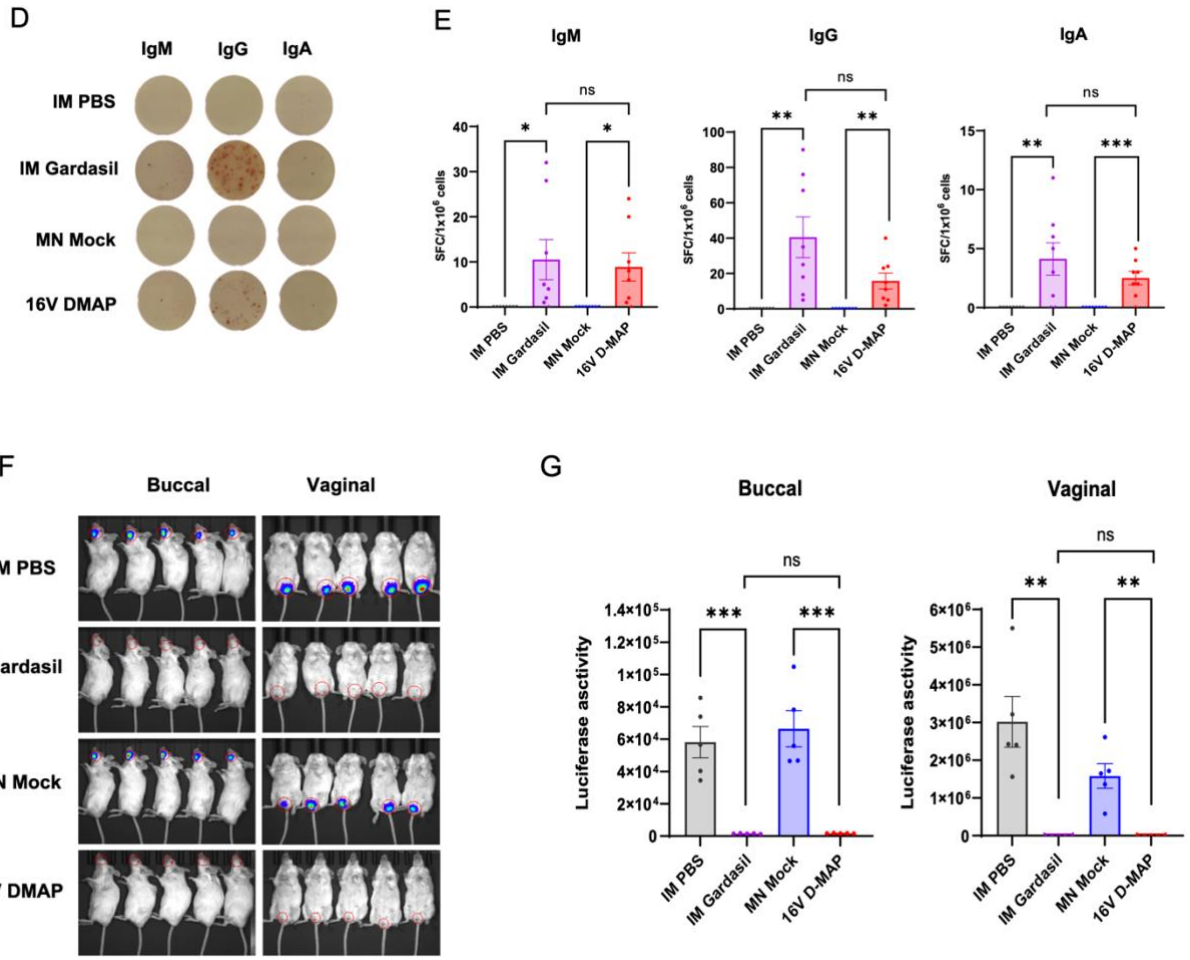

Figure 7. Assessment of long-term vaccine efficacy. (A) Schematic overview of immunization schedule and experimental design. Serum samples and bone marrow cells were harvested post-6 months final immunization for analysis. (B) HPV16-specific IgM, IgG, and IgA titers measured by ELISA. (C) Titers of HPV16-specific NAbs were measured by neutralization assay. (D) Representative ELISpot well images showing HPV16-specific IgM-, IgG-and IgA-secreting cells in BM. (E) Statistical analysis of antigen-specific ASCs per 10^6 BM cells. (F) Representative image of bioluminescence imaging of oral and vaginal mucosa areas of HPV16 PsV-FLuc challenged mice. (G) Statistical analysis of luciferase activity of oral and vaginal mucosa tissue. Data are presented as means ± SEM. ns> 0.05, * P<0.05, ** P ≤ 0.01, and **** P ≤ 0.0001 (unpaired t test).

4. Discussion

This study designed HPV16 vaccine utilizing DMAP delivery system. 16V DMAP were administrated on murine buccal mucosa and vaccine efficacy was evaluated by several immunological assays. Although oral buccal mucosa offers advantages such as low enzymatic activity and abundance of APCs, it presents physical challenges for microneedle application. The thick, moist, and elastic tissue can hinder sufficient penetration and reduce insertion efficiency, while high hydration level may accelerate premature microneedle dissolution. Despite these limitations, the DMAP used in this study were optimally engineered to be mechanically sturdy, allowing reliable penetration even in highly hydrated and elastic oral mucosa, preserve antigen structural integrity and enhance immunogenicity. Following administration, the DMAPs successfully delivered intact antigen to the local site and cervical drLNs, where antigen-specific B cells were activated. Robust humoral immune responses were elicited as demonstrated by marked GC formation, increased antigen-specific IgG and NAb titers and generation of LLPCs. Moreover, the vaccine-induced immune response conferred *in vivo* protection against HPV16 PsV infection and sustained immunity lasting up to six months post-final immunization.

Nevertheless, this study has several limitations. First, a direct comparison between I.M. and oral buccal mucosal routes was limited due to differences in antigen formulations. While the IM Gardasil vaccine contains a quadrivalent HPV VLP formulation (types 6, 11, 16, and 18) adjuvanted with amorphous aluminum hydroxyphosphate sulfate, the 16V-DMAP contained only HPV16 VLP combined with cholera toxin A1 (CTA1). Therefore, it is difficult to definitively assess or compare the immunogenic effects of the delivery route itself or the microneedle platform.

Second, the replacement of the CTA1 adjuvant is essential to ensure safety for human use. CTA1 has been reported to exhibit toxicity in both humans and animals. In fact, the intranasal influenza vaccine formulated with CTA1 was banned for human use due to its

association with Bell's palsy as a side effect, a symptom of facial paralysis, in vaccinated cohorts[57]. Additionally, nasal administration of CTA1 in mice caused damage to the olfactory system[58]. As a safer alternative, cholera toxin B subunit (CTB), a non-toxic subunit that lacks the enzymatic activity of CTA1, has been suggested. CTB has been proven to be safe and effective as an adjuvant in human clinical applications[59].

Third, although the aim of this study was to induce mucosal IgA responses, the 16V-DMAP failed to elicit antigen-specific IgA production in both serum and vaginal wash samples of immunized mice. This outcome may be attributed to technical limitations, such as the low sensitivity of the ELISA or suboptimal specificity of the detection antibodies used. Alternatively, insufficient antigen dosing or non-optimal adjuvant formulation may have hindered IgA induction. Despite the failure to induce mucosal IgA, a robust systemic IgG response was observed. This may be due to the anatomical characteristics of the murine oral buccal mucosa. The murine buccal mucosa is estimated to be approximately 200 μm thick[60], whereas the DMAP microneedles used in this study were 550 μm in length. Thus, it is likely that the microneedles penetrated beyond the submucosa and into the underlying muscle layer. This deeper delivery could have mimicked intramuscular immunization which typically favors strong serum IgG responses. However, the application of DMAP to the oral buccal mucosa of larger animals, such as pigs and non-human primates, whose buccal mucosa thickness ranges from 400 to 600 μm, may be more suitable for mucosal delivery. In particular, given that the human buccal mucosa is approximately 3290 μm thick, buccal administration is expected to result in more effective stimulation of mucosal immunity.

Interestingly, a previous study investigating fiber microneedle lengths (either 300 μm or 800 μm) applied to the oral buccal mucosa demonstrated that the longer microneedles promoted a more balanced Th1/Th2 immune response[61]. These findings suggest that needle length is a critical factor influencing local immune activation, potentially by determining

accessibility of tissue layers and APCs. Therefore, further optimization of DMAP length may serve as an effective strategy to enhance mucosal IgA responses. Moreover, a detailed analysis of the oral buccal mucosal immune environment—particularly focusing on Langerhans cells (LCs) and other local APC subsets—would provide deeper mechanistic insights into how DMAP-based delivery modulates immune responses.

Despite these limitations, the current study presents several advantages over prior approaches. First, the improved fabrication method enhanced antigen stability, a critical factor for maintaining immunogenicity during MN fabrication. Second, this research is the first to target oral buccal mucosa as a site for HPV vaccine delivery while prior researches have primarily focused on dermal administration[62, 63]. This study is also the first to strategically induce cross-mucosal immunity through oral mucosal vaccination, aiming to confer protective effects on distal mucosal sites such as the vaginal tissue. Lastly, the comprehensive evaluation from *in vitro* characterization to *in vivo* pseudovirus challenge provide thorough validation of the immunogenicity and protective efficacy of DMAP system.

5. Conclusion

In this study, dissolving microneedle array patch (DMAP)-based vaccine platform was developed for oral buccal mucosal delivery of HPV16 VLP. The goal was to establish a non-invasive strategy capable of eliciting systemic and mucosal immune responses against HPV. The results demonstrated that the 16V-DMAP successfully penetrated the oral mucosa and delivered antigen to induce robust HPV-specific IgG responses in mice. Although mucosal IgA induction was not achieved under the current formulation, the systemic immune response was comparable to that induced by conventional intramuscular vaccination, highlighting the potential of this platform as a viable alternative.

Overall, the findings of this study suggest that oral buccal microneedle vaccination represents a promising strategy for next-generation HPV vaccines. Furthermore, this platform is expected to be applicable to vaccines targeting other mucosa-invading pathogens. These results highlight the feasibility of site-specific microneedle immunization for cancer prevention and emphasize the importance of elucidating tissue-specific antigen uptake and cross-mucosal immune mechanisms. This work also lays a foundation for the future development of multivalent HPV microneedle vaccines targeting mucosal tissues.

References

1. Liao CI, Francoeur AA, Kapp DS, Caesar MAP, Huh WK, Chan JK. Trends in Human Papillomavirus-Associated Cancers, Demographic Characteristics, and Vaccinations in the US, 2001-2017. *JAMA Netw Open.* Mar 1 2022;5(3):e222530.
2. Kombe Kombe AJ, Li B, Zahid A, et al. Epidemiology and Burden of Human Papillomavirus and Related Diseases, Molecular Pathogenesis, and Vaccine Evaluation. *Front Public Health.* 2020;8:552028.
3. Burd EM. Human papillomavirus and cervical cancer. *Clin Microbiol Rev.* Jan 2003;16(1):1-17.
4. Petca A, Borislavschi A, Zvanca ME, Petca RC, Sandru F, Dumitrascu MC. Non-sexual HPV transmission and role of vaccination for a better future (Review). *Exp Ther Med.* Dec 2020;20(6):186.
5. Harper DM, DeMars LR. HPV vaccines – A review of the first decade. *Gynecologic Oncology.* 2017/07/01/ 2017;146(1):196-204.
6. Xi LF, Koutsky LA, Castle PE, et al. Relationship between cigarette smoking and human papilloma virus types 16 and 18 DNA load. *Cancer Epidemiol Biomarkers Prev.* Dec 2009;18(12):3490-3496.
7. Markowitz LE, Gee J, Chesson H, Stokley S. Ten Years of Human Papillomavirus Vaccination in the United States. *Acad Pediatr.* Mar 2018;18(2s):S3-s10.
8. Pimenoff VN, Gray P, Louvanto K, et al. Ecological diversity profiles of non-vaccine-targeted HPVs after gender-based community vaccination efforts. *Cell Host & Microbe.* 2023/11/08/ 2023;31(11):1921-1929.e1923.
9. Giuliano AR, Anic G, Nyitray AG. Epidemiology and pathology of HPV disease in males. *Gynecologic Oncology.* 2010;117(2):S15-S19.
10. Gravitt PE, Winer RL. Natural History of HPV Infection across the Lifespan: Role of Viral Latency. *Viruses.* 2017;9(10):267.
11. Piña-Sánchez P. Human Papillomavirus: Challenges and Opportunities for the Control of Cervical Cancer. *Arch Med Res.* Dec 2022;53(8):753-769.
12. Rosalik K, Tarney C, Han J. Human Papilloma Virus Vaccination. *Viruses.* Jun 8 2021;13(6).
13. Ali H, Guy RJ, Wand H, et al. Decline in in-patient treatments of genital warts among young Australians following the national HPV vaccination program. *BMC Infect Dis.* Mar 18 2013;13:140.
14. Guo F, Adekanmbi V, Hsu CD, Berenson AB. Incidence of human papillomavirus-related cancers among males and females aged 15-34 years in the United States. *JNCI Cancer Spectr.* Mar 1 2023;7(2).
15. Kasahun AW, Zewdie A, Shitu S, Alemayehu G. Vaccine cold chain management practice and associated factors among health professionals in Ethiopia: systematic review and meta-analysis. *J Pharm Policy Pract.* Apr 12 2023;16(1):55.
16. Maneze D, Salamonson Y, Grollman M, Montayre J, Ramjan L. Mandatory COVID-19 vaccination for healthcare workers: A discussion paper. *Int J Nurs Stud.* Feb 2023;138:104389.
17. Yeung KHT, Kim E, Yap WA, et al. Estimating the delivery costs of COVID-19 vaccination using the COVID-19 Vaccine Introduction and deployment Costing (CVIC) tool: the Lao People's Democratic Republic experience. *BMC Med.* Jul 10 2023;21(1):248.
18. Ashok A, Brison M, LeTallec Y. Improving cold chain systems: Challenges and solutions. *Vaccine.* 2017/04/19/ 2017;35(17):2217-2223.

19. Schreckenberger C, Sethupathi P, Kanjanahaluethai A, et al. Induction of an HPV 6bL1-specific mucosal IgA response by DNA immunization. *Vaccine.* 2000/09/15/ 2000;19(2):227-233.
20. Gordon SN, Kines RC, Kutsyna G, et al. Targeting the vaginal mucosa with human papillomavirus pseudovirion vaccines delivering simian immunodeficiency virus DNA. *J Immunol.* Jan 15 2012;188(2):714-723.
21. Xing M, Hu G, Wang X, et al. An intranasal combination vaccine induces systemic and mucosal immunity against COVID-19 and influenza. *NPJ Vaccines.* Mar 21 2024;9(1):64.
22. Hossain MK, Ahmed T, Bhusal P, et al. Microneedle Systems for Vaccine Delivery: the story so far. *Expert Rev Vaccines.* Dec 2020;19(12):1153-1166.
23. Menon I, Bagwe P, Gomes KB, et al. Microneedles: A New Generation Vaccine Delivery System. *Micromachines (Basel).* Apr 14 2021;12(4).
24. Chang H, Chew SWT, Zheng M, et al. Cryomicroneedles for transdermal cell delivery. *Nat Biomed Eng.* Sep 2021;5(9):1008-1018.
25. Moawad F, Pouliot R, Brambilla D. Dissolving microneedles in transdermal drug delivery: A critical analysis of limitations and translation challenges. *Journal of Controlled Release.* 2025/07/10/ 2025;383:113794.
26. Lee JW, Park J-H, Prausnitz MR. Dissolving microneedles for transdermal drug delivery. *Biomaterials.* 2008;29(13):2113-2124.
27. Larrañeta E, McCrudden MT, Courtenay AJ, Donnelly RF. Microneedles: a new frontier in nanomedicine delivery. *Pharmaceutical research.* 2016;33:1055-1073.
28. Mistilis MJ, Joyce JC, Esser ES, et al. Long-term stability of influenza vaccine in a dissolving microneedle patch. *Drug Deliv Transl Res.* Apr 2017;7(2):195-205.
29. Norman JJ, Arya JM, McClain MA, Frew PM, Meltzer MI, Prausnitz MR. Microneedle patches: usability and acceptability for self-vaccination against influenza. *Vaccine.* Apr 1 2014;32(16):1856-1862.
30. Márquez-Graña C, Bryan K, Vucen S, O'Sullivan C. Development of a novel single-use microneedle design platform for increased patient compliance. *Procedia Manufacturing.* 2017/01/01/ 2017;13:1352-1359.
31. Kim Y, Park IH, Shin J, et al. Sublingual Dissolving Microneedle (SLDMN)-Based Vaccine for Inducing Mucosal Immunity against SARS-CoV-2. *Adv Healthc Mater.* Oct 2023;12(26):e2300889.
32. Menon I, Patil S, Bagwe P, et al. Dissolving Microneedles Loaded with Nanoparticle Formulation of Respiratory Syncytial Virus Fusion Protein Virus-like Particles (F-VLPs) Elicits Cellular and Humoral Immune Responses. *Vaccines (Basel).* Apr 18 2023;11(4).
33. Hovav AH. Dendritic cells of the oral mucosa. *Mucosal Immunol.* Jan 2014;7(1):27-37.
34. Anggraeni R, Ana ID, Wihadmadyatami H. Development of mucosal vaccine delivery: an overview on the mucosal vaccines and their adjuvants. *Clin Exp Vaccine Res.* Sep 2022;11(3):235-248.
35. Ferreira LEN, Franz-Montan M, Benso B, Gill HS. Microneedles for oral mucosal delivery - Current trends and perspective on future directions. *Expert Opin Drug Deliv.* Jul-Dec 2023;20(9):1251-1265.
36. Wu C, Yu Q, Huang C, Li F, Zhang L, Zhu D. Microneedles as transdermal drug delivery system for enhancing skin disease treatment. *Acta Pharmaceutica Sinica B.* 2024/12/01/ 2024;14(12):5161-5180.
37. Ma Y, Tao W, Krebs SJ, Sutton WF, Haigwood NL, Gill HS. Vaccine Delivery to the Oral Cavity Using Coated Microneedles Induces Systemic and Mucosal Immunity.

Pharmaceutical Research. 2014/09/01 2014;31(9):2393-2403.

38. Lanzavecchia A. Antigen-specific interaction between T and B cells. *Nature.* Apr 11-17 1985;314(6011):537-539.

39. Li M, Wang Y, Sun Y, Cui H, Zhu SJ, Qiu HJ. Mucosal vaccines: Strategies and challenges. *Immunol Lett.* Jan 2020;217:116-125.

40. Lobaina Mato Y. Nasal route for vaccine and drug delivery: Features and current opportunities. *Int J Pharm.* Dec 15 2019;572:118813.

41. Ng YH, Chalasani G. Role of secondary lymphoid tissues in primary and memory T-cell responses to a transplanted organ. *Transplant Rev (Orlando).* Jan 2010;24(1):32-41.

42. De Silva NS, Klein U. Dynamics of B cells in germinal centres. *Nat Rev Immunol.* Mar 2015;15(3):137-148.

43. Kalan U. Flowcytometric Assessment of B Cell Development and Functional Assays on B Cell Development. In: Rezaei N, ed. *Encyclopedia of Infection and Immunity*. Oxford: Elsevier; 2022:106-121.

44. Crotty S. T follicular helper cell differentiation, function, and roles in disease. *Immunity.* Oct 16 2014;41(4):529-542.

45. Wong RS-Y, Tan T, Pang AS-R, Srinivasan DK. The role of cytokines in wound healing: from mechanistic insights to therapeutic applications. *Exploration of Immunology.* 2025;5:1003183.

46. Olatunde AC, Hale JS, Lamb TJ. Cytokine-skewed Tfh cells: functional consequences for B cell help. *Trends Immunol.* Jun 2021;42(6):536-550.

47. Klasse PJ, Sattentau QJ. Occupancy and mechanism in antibody-mediated neutralization of animal viruses. *J Gen Virol.* Sep 2002;83(Pt 9):2091-2108.

48. Bachmann MF, Mohsen MO, Zha L, Vogel M, Speiser DE. SARS-CoV-2 structural features may explain limited neutralizing-antibody responses. *NPJ Vaccines.* Jan 4 2021;6(1):2.

49. Nguyen DC, Garimalla S, Xiao H, et al. Factors of the bone marrow microniche that support human plasma cell survival and immunoglobulin secretion. *Nature Communications.* 2018/09/12 2018;9(1):3698.

50. Halliley JL, Tipton CM, Liesveld J, et al. Long-Lived Plasma Cells Are Contained within the CD19(-)CD38(hi)CD138(+) Subset in Human Bone Marrow. *Immunity.* Jul 21 2015;43(1):132-145.

51. Koike T, Fujii K, Kometani K, et al. Progressive differentiation toward the long-lived plasma cell compartment in the bone marrow. *J Exp Med.* Feb 6 2023;220(2).

52. Lightman SM, Utley A, Lee KP. Survival of Long-Lived Plasma Cells (LLPC): Piecing Together the Puzzle. *Front Immunol.* 2019;10:965.

53. Möbs C, Schmidt T. Research Techniques Made Simple: Monitoring of T-Cell Subsets using the ELISPOT Assay. *Journal of Investigative Dermatology.* 2016/06/01/ 2016;136(6):e55-e59.

54. Veri N, Mutiah C, Dewita D, et al. The Effect of Duration of Use of Depomedroxyprogesterone Acetate on the Thickness of the Vaginal Epithelium of Mice. *Open Access Macedonian Journal of Medical Sciences.* 01/15 2021;9(A):73-77.

55. Zuercher AW, Jiang HQ, Thurnheer MC, Cuff CF, Cebra JJ. Distinct mechanisms for cross-protection of the upper versus lower respiratory tract through intestinal priming. *J Immunol.* Oct 1 2002;169(7):3920-3925.

56. Dan JM, Mateus J, Kato Y, et al. Immunological memory to SARS-CoV-2 assessed for up to 8 months after infection. *Science.* 2021;371(6529):eabf4063.

57. Mutsch M, Zhou W, Rhodes P, et al. Use of the inactivated intranasal influenza vaccine and

the risk of Bell's palsy in Switzerland. *N Engl J Med.* Feb 26 2004;350(9):896-903.

58. Fukuyama Y, Okada K, Yamaguchi M, Kiyono H, Mori K, Yuki Y. Nasal Administration of Cholera Toxin as a Mucosal Adjuvant Damages the Olfactory System in Mice. *PLoS One.* 2015;10(9):e0139368.

59. Taylor DN, Cárdenas V, Sanchez JL, et al. Two-year study of the protective efficacy of the oral whole cell plus recombinant B subunit cholera vaccine in Peru. *J Infect Dis.* May 2000;181(5):1667-1673.

60. Hong S, Lee J, Moon J, et al. Intravital longitudinal cellular visualization of oral mucosa in a murine model based on rotatory side-view confocal endomicroscopy. *Biomed Opt Express.* Aug 1 2022;13(8):4160-4174.

61. Creighton RL, Faber KA, Tobos CI, Doan M-A, Guo T, Woodrow KA. Oral mucosal vaccination using integrated fiber microneedles. *Journal of Controlled Release.* 2024/03/01/ 2024;367:649-660.

62. Kines RC, Zarnitsyn V, Johnson TR, et al. Vaccination with human papillomavirus pseudovirus-encapsidated plasmids targeted to skin using microneedles. *PLoS One.* 2015;10(3):e0120797.

63. Vo TP, Panicker G, Braz-Gomes K, et al. Enhanced Immunogenicity of Adjuvanted Microparticulate HPV16 Vaccines Administered via the Transdermal Route. *Pharmaceuticals.* 2022;15(9):1128.

Abstract in Korean

인유두종바이러스 감염 예방을 위한 구강 점막면역 마이크로니들 백신 전달체계 개발

인체유두종 바이러스(Human papillomavirus, HPV)는 자궁경부암 및 두경부암의 발병에 직접적으로 연관되어 있어 전 세계적으로 심각한 공중보건 위협 요인으로 인식되고 있다. 현재 HPV 예방법은 근육주사를 통한 백신 접종으로, 근육주사 백신 제제는 냉장 보관 및 유통이 필수적이며, 접종 시 의료인력이 필요하다는 점에서 자원이 부족한 개발도상국에 접근성이 제한된다. 이런 한계를 극복하기 위해 본 연구에서는 용해성 마이크로니들 패치(DMAP) 전달법 기반의 HPV 백신을 개발하였다. 본 전달방법은 냉장 보관이 필요 없으며, 자가 접종 가능성의 장점을 가진다. 접종 부위로는 항원제시세포가 풍부한 구강 점막을 전략적으로 선택하였다. 조건 최적화를 통해 HPV16 바이러스유사입자를 패치 내에 안정적으로 포함시키는 제작 공정을 확립하였고, 이는 면역원성 유도에 핵심적인 구조적 안정성을 효과적으로 보존하였다. 이렇게 제작한 백신을 마우스모델에 접종하여 면역원성을 평가하였을 때, DMAP에 탑재된 HPV16 VLP가 구강 점막과 림프절 내로 이동되며 항원특이적 B세포에 효과적으로 전달되어 마우스 모델에서 혈청 기반 보호, 종자중심 구조 형성, 장기 면역 기억 유도를 포함한 강력한 체액성 면역 반응이 유도가 됨을 확인할 수 있었다. 특히, 구강 점막을 통한 접종 방법은 HPV 주요 감염 부위인 구강 및 질 점막 모두에서 교차 점막 면역을 유도하는 효과를 보였다. 본 연구는 VLP기반 용해성 마이크로니들 백신을 활용한 구강 점막 백신 접종 전략의 실현 가능성과 유효성을 입증하며 .기존 근육주사제 HPV 백신의 대안으로서 접근성과 효과를 동시에 갖춘 백신 플랫폼의 가능성을 제시한다.

핵심되는 말 : 인체유두종바이러스, 마이크로니들, 백신, 점막 면역, 체액성 면역